Talanta 212 (2020) 120798

Contents lists available at ScienceDirect

Talanta

journal homepage: www.elsevier.com/locate/talanta

Synergistic amplification effect for electrochemiluminescence immunoassay based on dual coreactants coupling with resonance energy transfer

Jing Wang*,[1], Hongxiang Wang[1], Weining Cao, Qianqian Zhang, Wenying Zhong**

Key Laboratory of Biomedical Functional Materials, School of Science, China Pharmaceutical University, Nanjing, 210009, China

ARTICLE INFO

Keywords:
Electrochemiluminescence
Resonance energy transfer
Dual coreactants
Silver nanoparticles
Graphite carbon nitride

ABSTRACT

Sensitive electrochemiluminescence (ECL) bioanalysis could be achieved by exploring the amplification principle or strategy. This work described the first proof-of-concept study for coupling dual coreactants ($K_2S_2O_8$ and H_2O_2) with localized surface plasmon resonance (LSPR) of silver nanoparticles (AgNPs) enhancement as an effective signal amplification strategy for ECL immunosensor. Specifically, AgNPs as an excellent conductor and nanocarriers were employed as the antibody (Ab_2) immobilization film on the glassy carbon electrode (GCE) for the subsequent sandwich-type immunoreaction between the target protein and antibody (Ab_1)-g-C_3N_4 resulted in the ECL generation. On the one hand, due to the perfect overlap between the plasmon absorption spectrum of AgNPs and the ECL emission spectrum of g-C_3N_4, a plasmon-enhanced ECL phenomenon was proved in g–C_3N_4–AgNPs system result from high efficient energy transfer. On the other hand, it was validated that the ECL signal of the constructed biosensor was greatly strengthened by $K_2S_2O_8$ and H_2O_2 as dual coreactants, which was ca. 3.5 and 7 times stronger than that of $K_2S_2O_8$ or H_2O_2 as an individual coreactant, respectively. Consequently, this synergistic amplified ECL immunosensor performed well with great stability and repeatability for squamous cell carcinoma antigen (SCCA) detection in the range from 0.001 to 1000 ng mL^{-1}. Considering the favorable analytical feedback in actual serum samples assay, this proposed method indicates a great potential for bioassay application.

1. Introduction

As a powerful and promising analytical method, electrochemiluminescence (ECL) has attracted numerous researchers' interest as a result of its remarkable advantages including low background, high sensitivity and requirements without excitation light source [1]. ECL immunoassay, based on highly specific molecular recognition of antigens by antibodies and the inherent advantages of ECL, has been recognized as a powerful analytical technique for sensitive and specific detection in bioanalysis [2,3]. Graphite carbon nitride (g-C_3N_4) is a novel two-dimensional semiconductor nanomaterial as a fascinating ECL emitter, which has attracted extensive attention due to its advantages over II − VI nanocrystals (NCs), such as a low energy band (~2.7 eV), large specific surface area and excellent biocompatibility [4,5]. These advantages make it particularly popular in designing the ECL immunosensors for the determination of Sudan I, carcinoembryonic antigen (CEA) and concanavalin A [6–8]. Nevertheless, the g-C_3N_4 nanosheets still suffer from weak emission in comparison to the conventional luminescent reagents, which may restrict their analytical applications. Thus, it is very significant to find a way to increase the ECL emission of g-C_3N_4.

The application of coreactants is an effective pathway to amplify ECL signal. In modern ECL systems, the ECL of luminophore typically requires the involvement of coreactants, which could help to overcome either the limited potential window of a solvent or poor anion or cation stability [9]. Coreactants such as hydrogen peroxide (H_2O_2), potassium persulfate ($K_2S_2O_8$) and O_2 have been the most frequently utilized to enhance the ECL responses by the generation of free radicals [10,11]. Lately, Xu's group first reported a convenient and effective way to greatly enhance ECL emissions of TiO_2 nanotubes by adding H_2O_2 and $K_2S_2O_8$ as dual coreactants simultaneously [9]. The intermediates hydroxyl radical (OH·) from H_2O_2 and the sulfate radical anion ($SO_4^{\cdot-}$) from $S_2O_8^{2-}$ could interact with each other and facilitate the production of excited states of nanomaterials, which displayed the increase of ECL intensity by several times in comparison to that of the biosensor with individual coreactant. Then, Dang et al. proposed a signal

* Corresponding author.
** Corresponding author.
E-mail addresses: wangjing@cpu.edu.cn (J. Wang), wyzhong@cpu.edu.cn (W. Zhong).
[1] These authors equally contributed to this work.

https://doi.org/10.1016/j.talanta.2020.120798
Received 28 September 2019; Received in revised form 18 January 2020; Accepted 29 January 2020
Available online 01 February 2020
0039-9140/

amplified ECL sensor by using dual coreactants (O_2 and $K_2S_2O_8$) and porous quantum dots towards the detection of oxytetracycline [12]. Inspired by this, we expect that the application of dual coreactants system could also dramatically promote the ECL emission of g-C_3N_4.

In recent years, ECL resonance energy transfer (ECL-RET) mechanism has been one of the most interesting protocols to enhance the ECL response for highly sensitive biosensors develop [13,14]. In ECL-RET system, the greatest overlap of the emission spectrum of donor and absorption spectrum of acceptor as well as the right separation distance between the donor and acceptor could cause the effective energy transfer [15]. Among various efforts, the plasmonic nanoparticles (Au, Ag, and Pt nanoparticles) have been widely investigated as the acceptor in the ECL-RET system for their localized surface plasmon resonance (LSPR) effect, which could enhance the local electromagnetic field and thus increase the emission intensity of the ECL donor [16]. Base on the excellent AuNPs plasmon-enhancement of ECL intensity, its rapid evolution has witnessed the tremendous advances of its bioanalytical applications in establishing various ECL-RET sensing platforms for detection of protein, nucleic acid and some ions [17–21]. Compared with AuNPs, AgNPs possess a very different dielectric function and exhibit a stronger plasmon resonance, which has manifested that Ag-based systems could offer larger influence than those provided by Au assemblies [22]. Coincidentally, the plasmon band of AgNPs greatly overlaps with the emission spectrum of g-C_3N_4, thereby making them a suitable donor–acceptor pair for the ECL-RET. Obviously, of particular interest here is the possibility of introducing Ag-based LSPR into the g-C_3N_4 ECL platform to exploit the improved signaling for advanced ECL bioassay application.

With special research attention on increasing the ECL intensity for sensitive sensing, this work presented a synergistic effect of dual coreactants and energy transfer between AgNPs and g-C_3N_4 for the realization of the highly sensitive detection of squamous cell carcinoma antigen (SCCA). As cancer biomarker, SCCA is a subtype of tumor-associated antigen TA-4, which abnormal concentration is closely related to several types of diseases, such as lung cancer, esophageal cancer and cervical cancer [23–25]. Nowadays, there have been some efforts in monitoring SCCA including radioimmunoassay, enzyme-linked immunosorbent assay (ELISA) and chemical immunoassay [26–28]. However, accurate, sensitive and wide-linear range SCCA detection is still of critical urgency for early diagnosis. In this protocol, we successfully constructed a novel synergy effect-based sandwich ECL SCCA immunoassay. Specifically, as shown in Scheme 1, the glassy carbon electrode (GCE) was decorated with AgNPs film, followed by the modification of SCC-antibody (Ab_2). In the presence of target, the prepared g-C_3N_4/Ab_1 conjugates as ECL emitter immobilized onto the modified electrode via formation of sandwich-type immune complexes. At the optimized dual coreactants conditions, on the basis of well energy matching, we experimentally confirmed that the LSPR of AgNPs could largely enhance the ECL performance of g-C_3N_4 because of highly efficient energy transfer. Meanwhile, the active intermediates OH· and $SO_4\cdot^-$ could be generated from the interaction between H_2O_2 and $K_2S_2O_8$, which further greatly promote the ECL signal. As such, this synergy effect amplified ECL immunoassay could be developed for the sensitive and specific detection of cancer marker SCCA and to the best of our knowledge has never been reported. It is worth noting that the operating principle of this study could be extended as a general protocol for other targets of interest.

2. Experimental

2.1. Reagents and apparatus

SCCA antigen, anti-SCCA McAb$_1$ (Ab_1), McAb$_2$ (Ab_2) and prostate specific antigen (PSA) were obtained from Shanghai Linc-Bio Science Co. LTD. (Shanghai, China). Alapha fetoprotein (AFP), neuron specifific enolase (NSE), carcinoembryonic antigen (CEA) were purchased from Key GEN Biotech. (Nanjing, China). Silver nitrate was obtained from Nanjing Chemical Reagent Company (Nanjing, China). N-hydroxysuccinimide (NHS), N-(3-(dimethylamino) propyl)-N′-ethyl-carbodiimide hydro-chloride (EDC), bovine serum (BSA) and Tween-20 were all obtained from Sigma-Aldrich Chem. Co. (St. Louis, MO, USA). 0.1 M phosphate-buffered solution (PBS, pH 7.4) prepared containing 0.1 M NaCl. All other chemicals of analytical grade were used as received without further purification. Ultrapure water (Mill-Q, Millipore, 18.2 MΩ cm resistivity) was used throughout the experiments.

The electrochemical measurements were recorded with CHI 660A electrochemical workstation (Shanghai CHI Instruments Co., China) at room temperature. Electrochemical impedance spectroscopy (EIS) was also performed with CHI 660A electrochemical workstation in a 10 mM $K_3Fe(CN)_6/K_4Fe(CN)_6$ (1 : 1) mixture with 1.0 M KCl as the supporting electrolyte, using an alternating current voltage of 5.0 mV, within the frequency range of 10^{-2}-10^6 Hz.

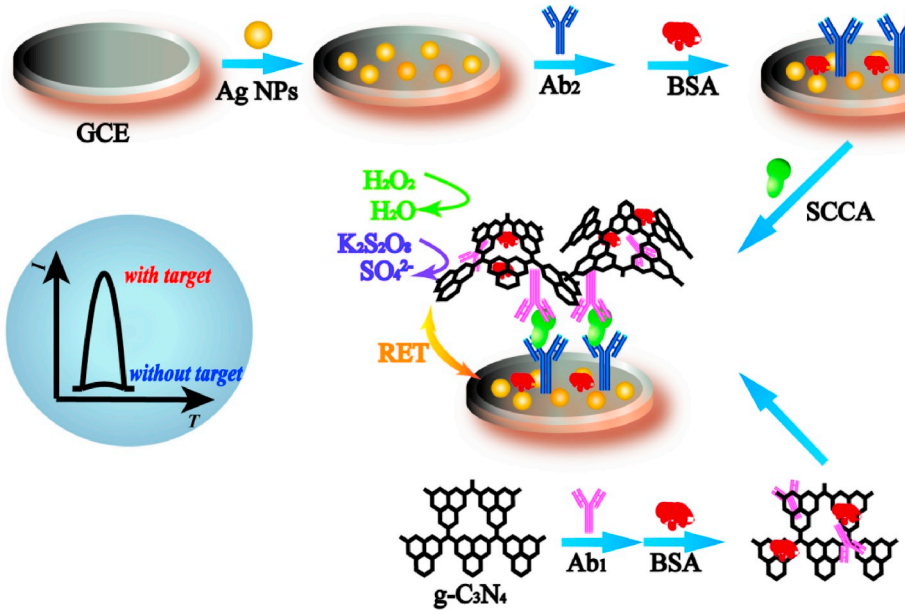

Scheme 1. Schematic illustration for the fabrication of the ECL immunosensor.

The ECL emission measurements were conducted on a Home-made ECL analyzer (assisted with CHI-660A electrochemical station). The spectral width of the photomultiplier tube (PMT) was 350–650 nm, and the voltage of the PMT was set at −800 V in the process of detection. The experiments were carried out with a three-electrode system, which used a GCE of 3 mm as working electrode, a platinum wire as auxiliary electrode, and a saturated calomel electrode (SCE) as reference electrode.

The UV–vis absorption spectrum was obtained on a UV-1800 photospectrometer (Shimadzu Co., Kyoto, Japan). Fourier transform infrared (FT-IR) spectra were performed with an IRAffinity-1S spectrophotometer (Shimadzu Co., Kyoto, Japan). Transmission electron microscopy (TEM) image was acquired on a JEOL model 2000 instrument operating at 200 kV accelerating voltage.

2.2. Synthesis of carboxylated g-C_3N_4, AgNPs and gold nanoparticles (AuNPs)

Carboxylated g-C_3N_4 was prepared in accordance with the reported methods with some slight modifications [29]. The basic steps are as follows: 5.0 g of melamine powder was added into a covered ceramic crucible. Then it was heated to 600 °C for 4 h and kept at this temperature for another 4 h in air. After naturally cooling to room temperature, the yellow g-C_3N_4 product was ground to powder for further use. And then, 1 g of bulk g-C_3N_4 were put into mixed acid (H_2SO_4:HNO_3 = 3:1, volume ratio), sonicating for 12 h to get the g–C_3N_4–COOH nanosheets. After that, the product was centrifuged and washed with ultrapure water until the pH reached 7. Finally, the carboxylated g-C_3N_4 was centrifuged with water and dried 12 h under 35 °C.

Colloidal AgNPs with an average diameter of 25 nm were synthesized referred to the previous report with slight modification [30]. In a typical synthesis, 100 mL of 1 mM $AgNO_3$ was heated in the water bath at 90 °C. Then, 3 mL of 1% sodium citrate aqueous solution was added to the solution drop by drop under magnetic stir. The reaction solution was further refluxed for 15 min at 90 °C with stirring until the color of the solution turned to yellow, followed by cooling to room temperature. The product was centrifuged and washed with ultrapure water for three times. Finally, the precipitate was redispersed in ultrapure water and stored at 4 °C.

Prior to experiment, all glasswares were cleaned thoroughly with aqua regia (3:1 in volume for HCl and HNO_3) for 12 h and thoroughly washed with ultrapure water. The AuNPs are synthesized according to the reference with the following steps [31]: 0.863 mL of 1.0% $HAuCl_4{\cdot}4H_2O$ (mass fraction, 0.024 mol L^{-1}) was primarily added into 94.138 mL of boiling water, and then immediately following 5.0 mL 1.0% trisodium citrate dihydrate (mass fraction, 0.034 mol L^{-1}) was added into the boiled reaction solution, with the solution kept boiling for 30 min and cooled down to room temperature. Also, the diameters of synthetic AuNPs are around 25 nm.

2.3. Preparation of g-C_3N_4/Ab_1 conjugates

The g-C_3N_4/Ab_1 conjugates were prepared through the reaction between activated carboxyl and amino of antibody [32]. In brief, 1 mL of prepared carboxylated g-C_3N_4 was activated with 1 mL 400 mM EDC and 100 mM NHS mixture for 6 h under vigorous stirring at room temperature, followed by thoroughly rinsing with PBS buffer. To modify activated g-C_3N_4, 10 μL of 1 mg mL^{-1} Ab_1 was added and incubated at 4 °C for 12 h under continuous stirring. The precipitate was washed with PBS (pH 7.4) to remove the unreacted substrates, followed by dispersing into 500 μL of 10 mg mL^{-1} BSA to block the nonspecific binding sites for 30 min. After that, the produced conjugates were centrifuged and washed with PBS several times. Finally, the resulted g-C_3N_4/Ab_1 conjugates were centrifuged and redispersed in 1.0 mL PBS (pH7.4) buffer and stored at 4 °C for further use.

2.4. Fabrication of the ECL immunosensor

The schematic diagram of the fabrication of the g–C_3N_4–based sandwich ECL immunosensor was shown in Scheme 1. Firstly, the GCE was polished in sequential order with 1.0, 0.3, and 0.05 nm of alumina slurry, and then sonicated in ethanol and ultrapure water in turn. The GCE was modified by drop-casting 10 μL of as-prepared AgNPs solution onto their surface and dried slowly in the air. Owning to the abundant active sites on the fresh surface of pretreated GCE, the AgNPs could adsorb on it firmly. After drying, 10 μL of 50 μg mL^{-1} Ab_2 solution was coated onto the surface of the modified GCE via the chemical bonds between protein and AgNPs and incubated at 4 °C for 12 h. In order to block the nonspecific active binding sites, the acquired GCE/AgNPs-Ab_2 were immersed in 10 μL of 10 mg mL^{-1} BSA and incubated for 30 min at 37 °C. Subsequently, to remove the physical adsorbed BSA, the electrode was rinsed with PBST (0.1 M PBS with 0.05% Tween-20) for three times. Then, the gaining electrode was immersed in 10 μL of SCCA solution with different concentrations for 80 min at 37 °C, followed by the washing process using PBST. Finally, 10 μL of the prepared g-C_3N_4/Ab_1 conjugates was assembled on the formed GCE/AgNPs-Ab_2/SCCA for another incubation of 40 min at 37 °C to construct a sandwiched immunocomplex. The ECL immunosensor was finished after flushing with the washing buffer again, and the electrode was stored at 4 °C for further use.

2.5. Detection of SCCA

For the detection of target SCCA, the modified electrode was incubated with variable concentrations of SCCA, which could result in different ECL signaling for quantization. The ECL responses of each step of the assembly process were recorded in 0.1 M PBS (pH 7.4) containing 0.1 M $K_2S_2O_8$ and 60 mM H_2O_2 as dual coreactants. The linear scan potential was applied with a scan rate of 100 mV s^{-1}, and the voltage of the photomultiplier tube (PMT) was set at −800 V.

3. Results and discussion

3.1. Characterization of g-C_3N_4 and g-C_3N_4/Ab_1 conjugates and AgNPs

The morphological of g-C_3N_4 was characterized by TEM. As depicted in Fig. 1A, the prepared carboxylated g-C_3N_4 presented the thin lamellar structure. Due to its high specific surface, it is very beneficial for anchoring more antibodies to fabricate the ECL immunosensor. The FT-IR spectra ranging from 400 to 4000 cm^{-1} could display the specific characteristic of g-C_3N_4 in Fig. 1B. The bands located at 1238, 1317, 1406, 1460 and 1574 cm^{-1} could be ascribed to the C–N stretching vibration of heterocycle groups, and the peak at 1645 cm^{-1} could be related to the C=N stretching vibration binding. The absorption peak at 812 cm^{-1} is the characteristic of the breathing vibration of the tris-s-triazine unit [33]. In addition, the broadband between 3000 and 3500 cm^{-1} may be related to the primary and secondary amines and O–H stretching vibrations of water molecules, which implied a larger amount of water adsorbed in the carboxylated g-C_3N_4 [34]. Due to the abundant oxygen-containing groups, the carboxylated g-C_3N_4 exhibited very good dispersity in water. The peak at 1680 cm^{-1} is corresponding to the C=O stretching vibration of the carboxyl group, also indicating successful functionalization of the carboxyl group on g-C_3N_4.

In order to confirm the successful synthesis of g-C_3N_4/Ab_1 conjugates, the UV–vis spectroscopy of g-C_3N_4, Ab_1 and g-C_3N_4/Ab_1 conjugates were performed which were shown in Fig. 1C. As displayed in curve a, the characteristic absorption peak of g-C_3N_4 was at approximately 316 nm [28]. For pure anti-SCCA solution, there was one major peak at approximately 280 nm (curve b). When Ab_1 was immobilized on the surface of carboxylated g-C_3N_4, two peaks shown in curve c corresponded to the characteristic peaks of g-C_3N_4 and Ab_1, which confirmed that it is useful to combine carboxylated g-C_3N_4 and Ab_1

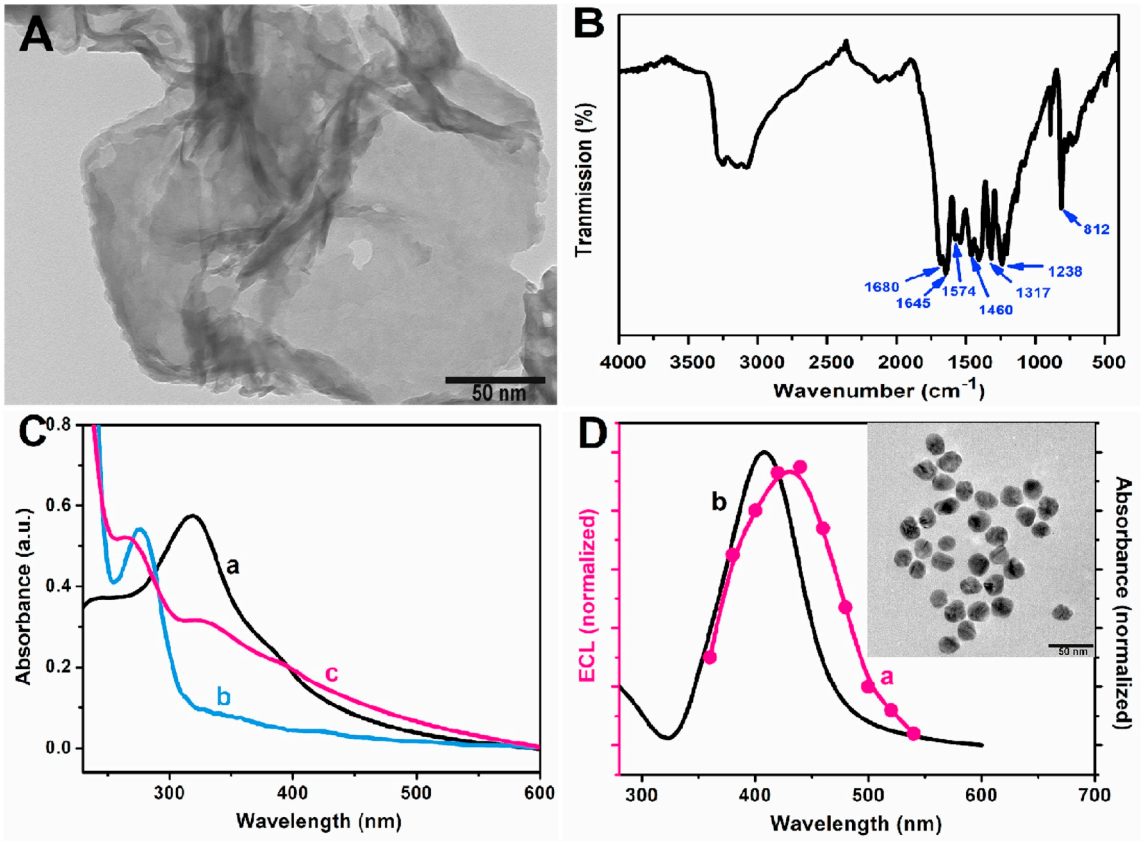

Fig. 1. A: The TEM image of carboxylated g-C_3N_4. B: The FT-IR spectra of carboxylated g-C_3N_4. C: The UV–vis absorbance spectra of (a) g-C_3N_4, (b) Ab_1 and (c) g-C_3N_4/Ab_1 conjugates. D: UV–vis absorption spectrum of AgNPs (black line) and ECL spectrum of g-C_3N_4 (red line) obtained through optical filters under a cyclic potential scan from 0 to −1.6 V. ECL detection buffer: 0.1 M PBS (pH 7.4) containing 0.1 mM $K_2S_2O_8$. Inset: the TEM of AgNPs. (For interpretation of the references to color in this figure legend, the reader is referred to the Web version of this article.)

with the activation agents of EDC and NHS.

The g-C_3N_4 exhibits high ECL activity in coreactant solutions of $S_2O_8^{2-}$ or H_2O_2 [28]. The curve a of Fig. 1D depicted the ECL spectrum of g-C_3N_4 by using $S_2O_8^{2-}$ as the coreactant, which matched closely with the characteristic PL spectrum of it [35]. The energy of the ECL peak (ca. 435 nm, 2.6 eV) basically coincided with the optical band gap energy (2.7 eV), indicating that ECL emission is the band gap luminescence. Worthy of note, it is clear that the ECL emission spectrum of g-C_3N_4 overlapped well with the UV–vis spectrum of AgNPs, which was characterized and shown in Fig. 1D curve b. A characteristic absorption peak centered at 410 nm was observed, which belongs to the plasmon resonance absorption of AgNPs. From the inset of Fig. 1D, the TEM image of AgNPs exhibited a homogeneous distribution and spherical shape with a diameter of 25 nm. Hence, this overlap ensured the feasibility of the RET between g-C_3N_4 and AgNPs at an appropriate distance during the ECL process.

3.2. Electrochemical and ECL behaviors of the immunosensor

To gain a better understanding of the fabrication processes of the ECL immunosensor, EIS as an effective tool was utilized to monitor the electrode interfacial feature. The experiments were performed with the electrodes modified with different substrates in 0.1 M PBS (pH 7.4) containing 0.1 M KCl and 5 mM $[Fe(CN)_6]^{4-}$/$[Fe(CN)_6]^{3-}$. The Nyquist plots of impedance for the stepwise modification processes were shown in Fig. 2A. The bare GCE exhibited a small semicircle portion with the Rct of 290 Ω at the high frequencies (curve a), which attributed to a free electron-transfer process. For the AgNPs modified GCE, the electrode exhibited a smaller semicircle domain with Rct value decreasing to 200 Ω (curve b), which revealed the faster electron transfer resistance of $[Fe(CN)_6]^{3-/4-}$ on GCE/AgNPs. It is also confirmed that the good conductivity of AgNPs increased the electron transfer capability. After the Ab_2 assembling (curve c), the BSA blocking (curve d) and subsequent stepwise immobilization of SCCA antigen (curve e) and g-C_3N_4/Ab_1 conjugates (curve f), the semicircle diameter and Rct value increased constantly from 669 Ω to 1679 Ω as the experiment proceeded. The reason for the resistance increase was that the nonconductive properties of the proteins could hinder the electron transfer process, which turned out the successful assembling of ECL immunosensor.

As exhibited in Fig. 2B, we also studied the developing processes of the amplified ECL bioassay through the stepwise ECL signal measuring. Under optimized conditions, a low ECL intensity of the GCE modified with AgNPs was presented in curve a, which provided a steady and almost negligible background detecting signal for the following fabrication procedure. Curve b suggested that the further anchoring of Ab_2 and blocking of BSA could not generate the ECL signal, instead a little impairing by the non-conductivity of protein. However, when g-C_3N_4 as electrochemiluminophores were introduced to the surface of GCE/Ag via the designed sandwich-type procedure, the ECL signal was improved considerably (curve c). Herein, we believed that there were at least three possible reasons for such conspicuous amplification of ECL signal: (1) Recently, some studies have demonstrated the ECL of semiconductor nanoparticles in dual coreactants was much stronger than that with single coreactant [36]. In this protocol, H_2O_2 was consequently introduced into the $K_2S_2O_8$-containing ECL solution, the ECL emission of g-C_3N_4 was enhanced greatly by this dual coreactant strategy. (2) The AgNPs modified on GCE not only acted as a good conductor to accelerate the electron transfer but also as nanocarriers to assemble more Ab_2 probe. (3) Besides, due to the good spectra overlap between the ECL emission spectra of g-C_3N_4 and absorption spectra of

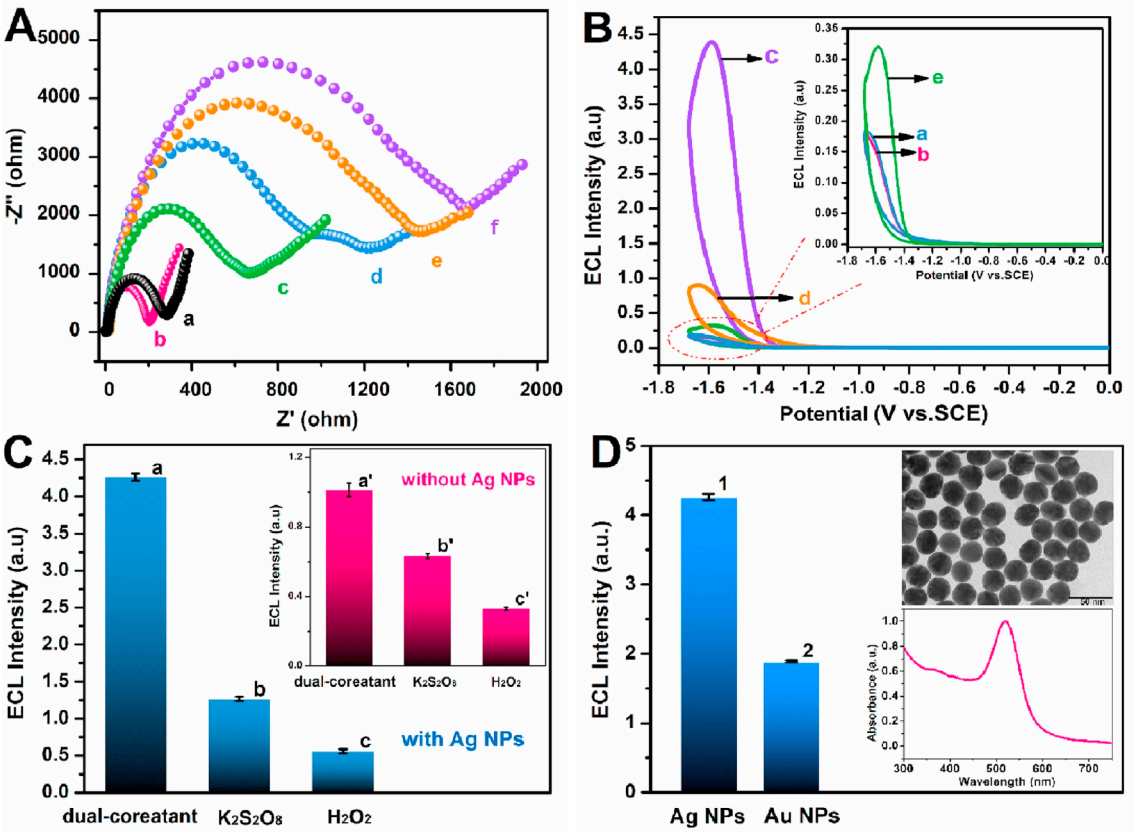

Fig. 2. A: EIS of (a) bare GCE, (b) GCE/AgNPs, (c) GCE/AgNPs-Ab_2, (d) GCE/AgNPs-Ab_2-BSA, (e) GCE/AgNPs-Ab_2-BSA/SCCA, (f) GCE/AgNPs-Ab_2-BSA/SCCA/Ab_1-g-C_3N_4. B: ECL response of the different modified electrode: (a) GCE/AgNPs, (b) GCE/AgNPs-Ab_2-BSA, (c) GCE/AgNPs-Ab_2-BSA/SCCA/Ab_1-g-C_3N_4, (d) GCE/Ab_2-BSA/SCCA/Ab_1-g-C_3N_4 in 0.1 M PBS (pH 7.4) containing 0.1 mM $K_2S_2O_8$ and 60 mM H_2O_2. (e) assembled GCE (c) in 0.1 M PBS without any coreactant. C: The ECL signals of GCE/AgNPs-Ab_2-BSA/SCCA/Ab_1-g-C_3N_4 in different medium (a) 0.1 mM $K_2S_2O_8$ and 60 mM H_2O_2, (b) 0.1 mM $K_2S_2O_8$, (c) 60 mM H_2O_2. Inset: the ECL signals of GCE/Ab_2-BSA/SCCA/Ab_1-g-C_3N_4 in different medium (a') 0.1 mM $K_2S_2O_8$ and 60 mM H_2O_2, (b') 0.1 mM $K_2S_2O_8$, (c') 60 mM H_2O_2. D: The ECL responses of (1) GCE/AgNPs-Ab_2-BSA/SCCA/Ab_1-g-C_3N_4 (2) GCE/AuNPs-Ab_2-BSA/SCCA/Ab_1-g- C_3N_4 in 0.1 M PBS containing 0.1 mM $K_2S_2O_8$ and 60 mM H_2O_2. Inset: TEM image and UV–vis absorption spectrum of AuNPs.

AgNPs and their appropriate separate distance, the highly efficient energy resonance transfer could occur and ECL signal could be significantly strengthened.

3.3. ECL enhancing mechanism of constructed immunosensor

According to some previous studies, $K_2S_2O_8$ or H_2O_2 were often applied to increase the ECL emission of g-C_3N_4 as its coreactant by the generation of free radicals [12]. Comparing with the curve c in Fig. 2B, it was evident that the ECL response of the same sandwich immunosensor in medium containing both $K_2S_2O_8$ and H_2O_2 was about approximately 14 times higher than that in medium without any coreactant (Fig. 2B curve e). The result indicated that the coreactant was one of the most vital elements that could hugely influence the electron transmission behavior of the reaction system. Additionally, the Xu's group has proved that the ECL intensity of semiconductor TiO_2 nanotubes and CdS nanocrystal film would effectively be enhanced by H_2O_2 and $K_2S_2O_8$ as dual coreactants [9]. The reason for this phenomenon was considered that the electrogenerated coreactant-related radical OH · (hydroxyl radical) could vastly promote the amount of sulfate radical anion (SO_4·$^-$) near the electrode surface. As expected, in our strategy, the ECL intensity of g-C_3N_4 showed a similar boosting when H_2O_2 and $K_2S_2O_8$ as dual coreactants.

To further verify this mechanism, the detection signals of ECL immunosensor modified with or without AgNPs were studied in the electrolyte with different coreactants. From Fig. 2C, it was apparently seen that the ECL intensity of two kind modified biosensors in dual coreactants were both found much stronger than those of in sole coreactant. Furthermore, when AgNPs were participated in assembling of the biosensor, the ECL signal in dual coreactants ascend to 3.5 and 7 times that of with single $K_2S_2O_8$ or H_2O_2, separately, which was higher than the same circumstance of biosensors absence of AgNPs. This suggested the synergistic effects of dual coreactants and AgNPs towards dramatically improved ECL signals.

On the basis of the above results, the possible reactions among g-C_3N_4, H_2O_2, and $S_2O_8^{2-}$ on GCE were described as follows:

(i) Electrochemical reduction

$$\text{g-}C_3N_4 + e^- \rightarrow \text{g-}C_3N_4\cdot^- \quad (1)$$

$$S_2O_8^{2-} + e^- \rightarrow SO_4^{2-} + SO_4\cdot^- \quad (2)$$

$$H_2O_2 + e^- \rightarrow OH^- + OH\cdot \quad (3)$$

(ii) Synergy effect of dual coreactants

$$SO_4\cdot^- + H_2O \rightarrow OH\cdot + HSO_4^- \quad (4)$$

or

$$OH\cdot + S_2O_8^{2-} \rightarrow SO_4\cdot^- + HSO_4^- + 1/2O_2 \quad (5)$$

(iii) ECL emission procedure

$$\text{g-}C_3N_4\cdot^- + SO_4\cdot^- \rightarrow \text{g-}C_3N_4^* + SO_4^{2-} \quad (6)$$

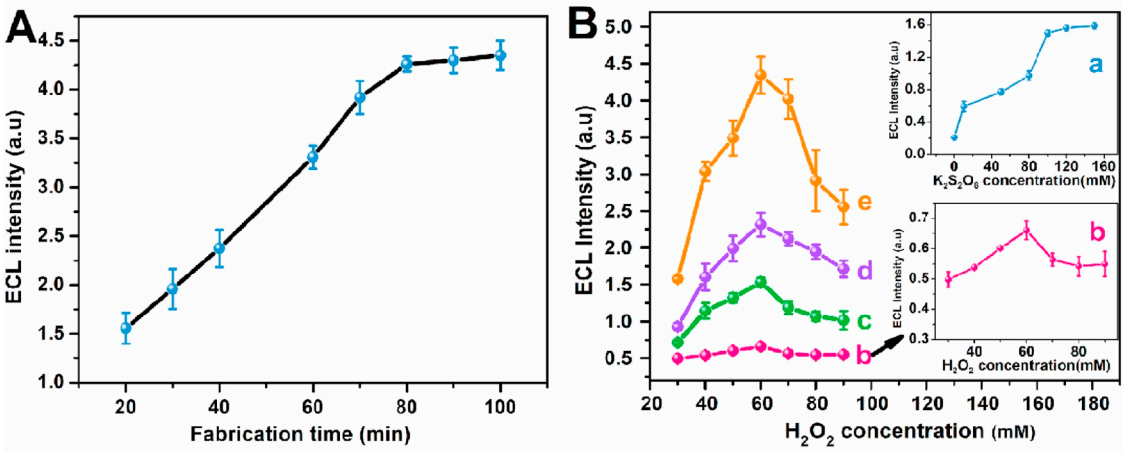

Fig. 3. A: Effects of the incubation time on the ECL intensity of immunosensor in 0.1 M PBS containing 0.1 M $K_2S_2O_8$ and 60 mM H_2O_2. B: Effects of the $K_2S_2O_8$ concentration (inset a) and $K_2S_2O_8$ fixed at (b) 0 mM, (c)10 mM, (d)50 mM and (e)100 mM with different concentrations of H_2O_2 (30, 40, 50, 60, 70, 80 and 90 mM) on the ECL intensity of immunosensor. The concentration of SCCA was 1 ng mL^{-1}.

$$g\text{-}C_3N_4^* \rightarrow g\text{-}C_3N_4 + h\upsilon \quad (7)$$

or

$$g\text{-}C_3N_4 + SO_4\cdot^- \rightarrow g\text{-}C_3N_4^+ + SO_4^{2-} \quad (8)$$

$$g\text{-}C_3N_4^+ + g\text{-}C_3N_4\cdot^- \rightarrow g\text{-}C_3N_4^* + g\text{-}C_3N_4 \quad (9)$$

As shown in equations (1)–(3), the electrochemical reduction concerned with g-C_3N_4, $K_2S_2O_8$ and H_2O_2. The pure g-C_3N_4 produced the anionic g-C_3N_4 radicals (g-$C_3N_4\cdot^-$), while the dual coreactants containing $K_2S_2O_8$ and H_2O_2 were degraded to SO_4^{2-}, $SO_4\cdot^-$, OH^- and OH ·. Meanwhile, the electron transfer rate increased in the presence of AgNPs based on its conductivity, which could promote the production of $SO_4\cdot^-$. Subsequently, equation (4) indicated that the sulfate ion reacting with H_2O formed OH·, which could expedite the degradation process of $S_2O_8^{2-}$ and further accelerate the $SO_4\cdot^-$ formation (Eq (2) and (5)). Finally, there are two patterns related to ECL emission. The g-$C_3N_4\cdot^-$ could react with $SO_4\cdot^-$and the excited state g-C_3N_4 (g-C_3N_4*) was produced (Eq (6)). Then the g-C_3N_4*returned to the ground state (g-C_3N_4) and the ECL phenomenon emerged (Eq (7)). Whereas another emission mode displayed in equations (8) and (9). The g-$C_3N_4^+$was produced by enabling pure g-C_3N_4 reacting with $SO_4\cdot^-$. The anionic g-C_3N_4 radicals further reacted with g-$C_3N_4^+$ and g-C_3N_4*generated [37,38]. Based on the above discussed, the ECL enhancement of the g-C_3N_4 by dual coreactants ascribed to the principal effect of $K_2S_2O_8$, the intermediate ($SO_4\cdot^-$) of which generated the excited states of g-C_3N_4. And OH· could facilitate electrochemical reduction and decomposition of $S_2O_8^{2-}$, which helped in the ECL signal amplification strikingly.

On the other hand, AgNPs also played a crucial role in enhancing the ECL emission. As shown in Fig. 2B curve d, the control experiment observed a much lower ECL enhancement of designed biosensor, which did not involve the AgNPs. The reason should be attributed to that AgNPs modified on GCE presented the advantages of large surface area, good biocompatibility and excellent electron transfer as many previous works reported [39]. What is more, thanks to the energy matching between the AgNPs and g-C_3N_4, AgNPs brought in outstanding performance for the influence of LSPR on the ECL emission of g-C_3N_4 in the view of the significantly large local electromagnetic field enhancement that located around the metal NPs. To demonstrate the superiority of the AgNPs in this construction of biosensor, we took the AuNPs with an average size of 25 nm into comparison. The TEM image showed that the synthesized AuNPs possessed good homogeneity (Fig. 4D inset). Alternatively, these AuNPs were used to replace the AgNPs in the electrode assembly process. In this case, after sandwich immunocomplex modified GCE by incubating with the same concentration of target, an obvious ECL signal diminution was shown in bar 2 of Fig. 2D, which only reached 37.8% of the value of AgNPs-based biosensor (bar 1). Since AuNPs are good conductors like AgNPs, this evident difference of signal responses could come from the efficiency of energy transfer between g–C_3N_4–AgNPs and g–C_3N_4–AuNPs system. For the efficient excitation of the LSPR, the overlap degree of the spectra between the ECL donor-acceptor pairs is essential. Fig. 2D inset also showed the AuNPs had a typical maximum absorption with the peak at ca. 520 nm. Apparently, this LSPR absorption of the AuNPs is mismatched with the ECL emission spectra of g-C_3N_4, which exhibited a lower efficiency of RET result in a much lower enhancement of corresponding ECL. These results validated the superior performance of AgNPs in this LRET-ECL biosensor. Taken together, these experimental results demonstrated that the overall amplified ECL response was based on the synergy effect of dual coreactants and the energy transfer between g-C_3N_4 and AgNPs.

3.4. Optimization of experimental conditions

In order to achieve better ECL performance of SCCA detection, the major experiment conditions that could affect the analytical results of the biosensor have been investigated, such as incubation time of immunoreaction and the concentration of H_2O_2 and $K_2S_2O_8$. The effect of incubation time on the response of the immunosensor was shown in Fig. 3A. With the increasing incubation time, the ECL values increased and then tended toward a plateau after 80 min, implying that immunoreaction reached an equilibrium state. Thus, 80 min was chosen as the optimal incubation time.

The effect of the concentration of $K_2S_2O_8$ and H_2O_2 on the ECL intensity of this biosensor was investigated. As illustrated in curve a of Fig. 3B, the ECL intensity increased rapidly while $K_2S_2O_8$ acting as the only coreactant with the concentration ranged from 0 to 100 mM. Moreover, the ECL intensity began a fairly steady climb while the concentration of $K_2S_2O_8$ was higher than 100 mM, because of the limitation of the electrode surface area. While, the effect of the concentration of H_2O_2 on the ECL intensity is shown in Fig. 3B, curve b. A gradual increase of the ECL signal with the increase of the amount of H_2O_2 from 0 mM to 60 mM. And a slight decrease appeared in the concentration higher than 60 mM as a result of the destruction of the redundant hydroxyl radicals. Since $K_2S_2O_8$ and H_2O_2 could demonstrate concurrent, it was very necessary to further discuss the effect of the relative amount of $K_2S_2O_8$ and H_2O_2 in one system. Specifically, the $K_2S_2O_8$ concentrations fixed at 10 mM (curve c), 50 mM (curve d) and 100 mM (curve e), the ECL intensity of the biosensors surged with the

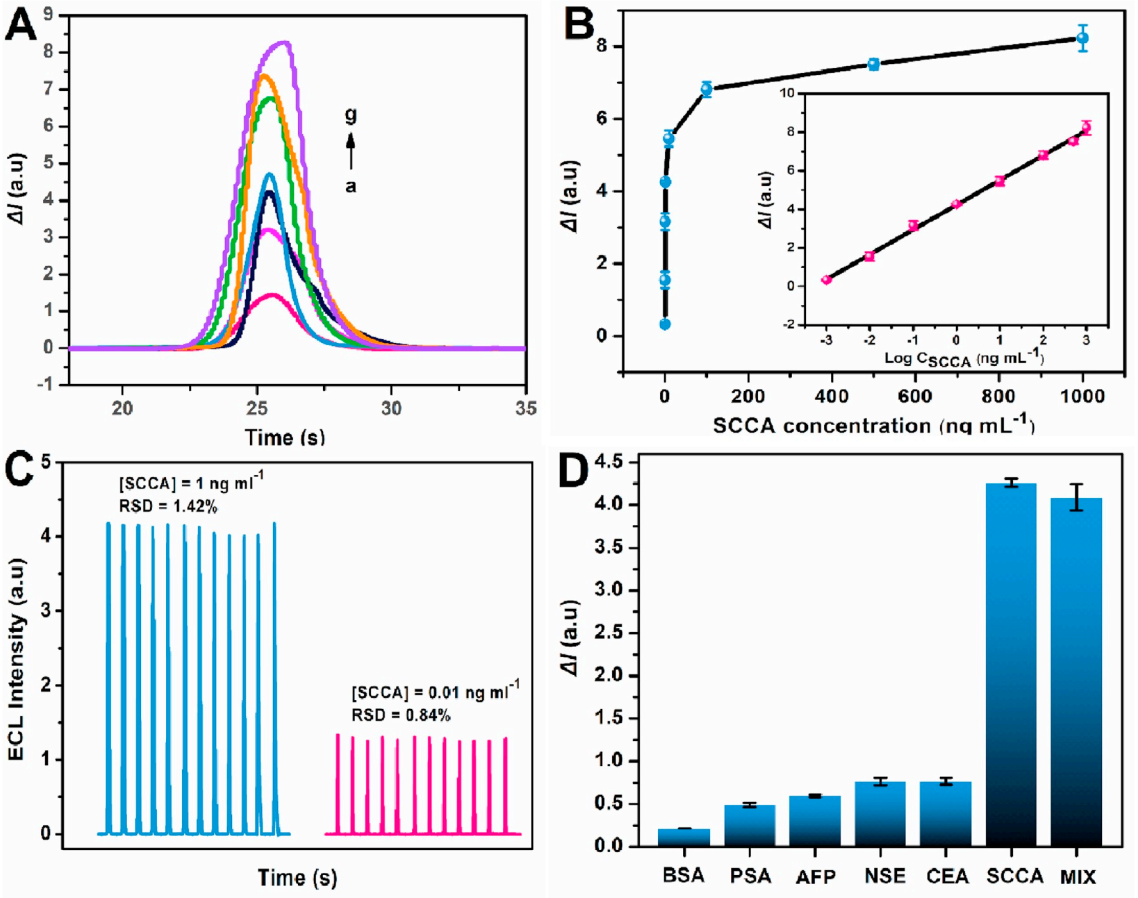

Fig. 4. A: The ECL responses of the immunosensors incubating SCCA with different concentrations (a–g): 0.001, 0.01, 0.1, 1, 10, 100, 500, 1000 ng mL^{-1}. B: Calibration curve of SCCA detection. Inset: Linear plot of the ECL intensity vs logarithmic concentration of SCCA, five measurements for each point. C: Stability of ECL emissions with 0.01 ng mL^{-1} and 1 ng mL^{-1} SCCA, respectively under continuous scanning for 12 cycles in PBS containing 0.1 M $K_2S_2O_8$ and 60 mM H_2O_2. D: Specifificity of the proposed immunosensor to SCCA (1 ng mL^{-1}) by comparing it to the interfering proteins at the 100 ng mL^{-1} level: BSA, PSA, AFP, NSE, CEA and the mixed sample. The error bars showed the standard deviation of five replicate determinations.

increase in the H_2O_2 concentrations and all reached the maximum at 60 mM. To sum up, after 80 min incubate reaction, the strongest ECL emission of the constructed immunosensor was achieved in 0.1 M PBS containing 0.1 M $K_2S_2O_8$ and 60 mM H_2O_2.

3.5. Performance of the immunosensor in SCCA detection

Since the ECL responses of the prepared immunosensor were related to the concentration of g-C_3N_4 nanocomposite controlled by the target, it is possible to quantitatively detect SCCA through the changes of ECL intensity. The synergistic amplified ECL assay of the biosensor was carried out under the optimized experimental conditions and was shown in Fig. 4A. It is clear that the ECL emission of g-C_3N_4 increased gradually along with changing the target SCCA concentration from 0.001 to 1000 ng mL^{-1} (curve a to curve g). And Fig. 4B illustrated a good linear relationship between the ECL intensity and the logarithmic concentration of SCCA. The linear equation was $\Delta I = 4.2305 + 1.2859 \log C_{SCCA}$ with the correlation coefficient was 0.9975. ΔI represents the degree of the ECL intensity change, $\Delta I = I - I_0$, where I and I_0 are the ECL intensity in the presence and absence of SCCA, respectively. Due to the synergy effect as stated above, the detection limit was estimated to be 0.49 pg mL^{-1} (S/N = 3) according to the previous literature [40]. In total, the results represented that this ECL immunosensor based on dual amplification strategy possessed excellent property in analyzing SCCA. Moreover, the comparisons to other reported methods in recent years were recorded in Table 1, which denoted this proposed ECL immunosensor exhibited a good outlook in precise measurement of SCCA with a lower detection limit and/or wider detection range.

3.6. Stability, selectivity and reproducibility of the immunosensor

Operational stability was one of the major concerns for the practical application of biosensors. Fig. 4C displayed the ECL emission with two different SCCA concentrations has a stable readout for signal collection under 12 cycle measurements. After the storage in pH 7.4 PBS in the refrigerator at 4 °C for 1 month, the biosensor showed quite satisfying stability, which retained about 96.5% of its initial response. Based on such high and stable ECL signals, this immunosensor was favorable for ECL assay.

In order to evaluate the selectivity of the immunosensor, the interference experiment was further studied by measuring the ECL responses to a serious of proteins, including BSA, PSA, AFP, NSE and CEA at the concentration of 100 ng mL^{-1}. As shown in Fig. 4D, the ECL responses from other proteins were much lower than that of 1 ng mL^{-1} SCCA, demonstrating that the ECL response was caused by the specific binding. What's more, the ECL intensity of a mixture containing 1 ng mL^{-1} SCCA and other interfering substrates at the concentration of 100 ng mL^{-1} was measured, which displayed that there was little difference with the result performed in the presence of only SCCA. All these results implied that the proposed immunoassay had acceptable selectivity without obvious interference from nonspecific adsorption.

In addition, to study the reproducibility of the ECL immunosensor, the same batches (intra-assay) and different batches (inter-assay) of five sensors were investigated under the same conditions. Analyzed from

Table 1
Comparison with other reported technologies for detection of SCCA.

Detection methods	Linear range (ng mL^{-1})	LOD (pg mL^{-1})	References
Sandwich electrochemical immunosensor	0.001–5	0.3	[41]
LSPR immunoassay	2.5–115	850	[42]
Label-free electrochemical immunosensor	0.01–100	5.5	[43]
Label-free electrochemical immunosensor	0.001–5	0.3	[44]
ECL immunosensor	0.001–1000	0.49	This work

Table 2
Determination of SCCA added in human blood serum (n = 5) with the developed immunosensor.

Serum samples	Added SCCA (ng mL^{-1})	Found SCCA (ng mL^{-1})	Relative standard deviation (%)	Recovery (%)
1	0.5	0.527	2.2	105.4
2	1.0	0.956	2.8	95.6
3	5.0	4.67	4.2	93.5
4	20	21.2	3.6	106.2

the experimental results, the relative standard deviations (RSD) of inter- and intra-assay were 2.9% and 4.1% respectively, which suggested an acceptable precision and reproducibility of the proposed protocol.

3.7. Analytical application of the immunosensor in real samples

To evaluate the practical application of this dual amplified ECL immunosensor, recovery testing was also examined by spiking target SCCA solution into 10% human serum. The spiked sample with different concentrations of SCCA was measured by the proposed method. As displayed in Table 2, the recoveries varied in the range of 93.5–106.2% and the RSDs were no more than 4.2%. Apparently, the satisfactory results made the proposed ECL biosensor for SCCA detection feasible to apply to the biology system.

4. Conclusion

In summary, a sensitive and sandwich ECL immunosensor for the detection of SCCA was developed, which was based on the synergistic effect of dual coreactants and AgNPs LSPR-induced enhancement of ECL mission from g-C_3N_4. Since the superior performance of this signal amplification strategy for ECL bioassay, the constructed immunosensor presented an excellent analytical performance for SCCA determination with high sensitivity, acceptable selectivity, reproducibility, and stability. Importantly, this work provided a new perspective for signal amplification of ECL biosensor with other emitters and exhibited a great potential application in the monitoring of other cancer markers by changing the recognition element.

Acknowledgements

This work was financially supported by the National Natural Science Foundation of China (no. 21775165), the China Postdoctoral Science Foundation (nos. 2015T80535), the Natural Science Foundation of Jiangsu Province (no. BK20161455), the College Students Innovation Project for the R&D of Novel Drugs (no. J1310032), and the 'Double First-Class' University project (no.CPU2018GY25).

References

[1] M.M. Richter, Electrochemiluminescence (ECL), Chem. Rev. 104 (2004) 3003–3036.
[2] X. Wang, H. Gao, H. Qi, Q. Gao, C. Zhang, Proximity hybridization-regulated immunoassay for cell surface protein and protein-overexpressing cancer cells via electrochemiluminescence, Anal. Chem. 90 (2018) 3013–3018.
[3] Y. Ai, X. Li, L. Zhang, W. Zhong, J. Wang, Highly sensitive electrochemi- luminescent immunoassay for neuron-specific enolase amplified by single-walled carbon nanohorns and enzymatic biocatalytic precipitation, J. Electroanal. Chem. 818 (2018) 257–264.
[4] G. Algara-Siller, N. Severin, S.Y. Chong, T. Bjorkman, R.G. Palgrave, A. Laybourn, M. Antonietti, Y.Z. Khimyak, A.V. Krasheninnikov, J.P. Rabe, U. Kaiser, A.I. Cooper, A. Thomas, M.J. Bojdys, Triazine-based graphitic carbon nitride: a two-dimensional semiconductor, Angew Chem. Int. Ed. Engl. 53 (2014) 7450–7455.
[5] Y.T. Liu, Q.B. Wang, J.P. Lei, Q. Hao, W. Wang, H.X. Ju, Anodic electrochemiluminescence of graphitic-phase C_3N_4 nanosheets for sensitive biosensing, Talanta 122 (2014) 130–134.
[6] W. Chen, X. Yao, X. Zhou, K. Zhao, A. Deng, J. Li, Electrochemiluminescence based competitive immunoassay for Sudan I by using gold-functionalized graphitic carbon nitride and Au/Cu alloy nanoflowers, Microchim. Acta 185 (2018) 275.
[7] Y. Jin, Q. Kang, X. Guo, B. Zhang, D. Shen, G. Zou, Electrochemical- signal-amplification strategy for an electrochemiluminescence immunoassay with g-C_3N_4 as tags, Anal. Chem. 90 (2018) 12930–12936.
[8] H. Sha, Y. Zhang, Y. Wang, H. Ke, X. Xiong, N. Jia, Electrochemiluminescence resonance energy transfer biosensor between the glucose functionalized MnO_2 and g-C_3N_4 nanocomposites for ultrasensitive detection of concanavalin A, Biosens. Bioelectron. 124–125 (2019) 59–65.
[9] P.P. Dai, T. Yu, H.W. Shi, J.J. Xu, H.Y. Chen, General strategy for enhancing electrochemiluminescence of semiconductor nanocrystals by hydrogen peroxide and potassium persulfate as dual coreactants, Anal. Chem. 87 (2015) 12372–12379.
[10] L.j. Xiao, Y.Q. Chai, R. Yuan, Y.L. Cao, H.J. Wang, L.J. Bai, Amplified electrochemiluminescence of luminol based on hybridization chain reaction and in situ generate co-reactant for highly sensitive immunoassay, Talanta 115 (2013) 577–582.
[11] H. Wang, Y. Song, Y. Chai, R. Yuan, High-sensitive electrochemiluminescent analysis based on co-reactive high-molecular polymer and dual catalysis to generate oxygen in situ, Anal. Chim. Acta 1081 (2019) 65–71.
[12] X. Dang, M. Sun, A. Sinha, J. Niu, H. Zhao, Coupling O_2 and $K_2S_2O_8$ dual co-reactant with Fe-N-C modified electrode for ultrasensitive electrochemi- luminescence signal amplification, Chem. Select 4 (2019) 1673–1680.
[13] J. Wang, W.W. Zhao, H. Zhou, J.J. Xu, H.Y. Chen, Amplified electrochemi- luminescence detection of DNA-binding protein based on the synergy effect of electron and energy transfer between CdS nanocrystals and gold nanoparticles, Biosens. Bioelectron. 41 (2013) 615–620.
[14] Y. Zhou, Y.Q. Yu, Y.Q. Chai, R.Yuan, Electrochemical synthesis of silver nanoclusters on electrochemiluminescent resonance energy transfer amplifification platform for Apo-A1 detection, Talanta 181 (2018) 32–37.
[15] J. Wang, Y. Shan, W.W. Zhao, J.J. Xu, H.Y. Chen, Gold nanoparticle enhanced electrochemiluminescence of CdS thin films for ultrasensitive thrombin detection, Anal. Chem. 83 (2011) 4004–4011.
[16] D. Wang, Y. Li, Z. Lin, B. Qiu, L. Guo, Surface-enhanced electrochemi- luminescence of Ru@SiO2 for ultrasensitive detection of carcinoembryonic antigen, Anal. Chem. 87 (2015) 5966–5972.
[17] J.X. He, K. Wang, D. He, Y. Wang, Y. Mao, H. Shi, L. Wen, A highly sensitive electrochemiluminescence assay for protein kinase based on double-quenching of graphene quantum dots by G-quadruplex-hemin and gold nanoparticles, Biosens. Bioelectron 70 (2015) 54–60.
[18] H. Ke, H. Sha, Y. Wang, W. Guo, X. Zhang, Z. Wang, C. Huang, N. Jia, Electrochemiluminescence resonance energy transfer system between GNRs and Ru $(bpy)_3^{2+}$: application in magnetic aptasensor for beta-amyloid, Biosens. Bioelectron. 100 (2018) 266–273.
[19] M.X. Li, Q.M. Feng, Z. Zhou, W. Zhao, J.J. Xu, H.Y. Chen, Plasmon-enhanced electrochemiluminescence for nucleic acid detection based on gold nanodendrites, Anal. Chem. 90 (2018) 1340–1347.
[20] B. Babamiri, A. Salimi, R. Hallaj, Switchable electrochemiluminescence aptasensor coupled with resonance energy transfer for selective attomolar detection of Hg2+ via CdTe@CdS/dendrimer probe and Au nanoparticle quencher, Biosens. Bioelectron. 102 (2018) 328–335.
[21] Y.M. Lei, W.X. Huang, M. Zhao, Y.Q. Chai, R. Yuan, Y. Zhuo, Electrochemi- luminescence resonance energy transfer system: mechanism and application in ratiometric aptasensor for lead ion, Anal. Chem. 87 (2015) 7787–7794.
[22] W. Zhao, Z. Jusys, R.J. Behm, Complete quantitative online analysis of methanol electrooxidation products via electron impact and electrospray ionization mass spectrometry, Anal. Chem. 84 (2012) 5479–5483.
[23] K. Kagohashi, H. Satoh, K. Kurishima, K. Kadono, H. Ishikawa, M. Ohtsuka, K. Sekizawa, Squamous cell carcinoma antigen in lung cancer and nonmalignant respiratory diseases, Lung Canc. 186 (2008) 323–326.
[24] L. Zhao, H. Han, Z. Ma, Improved screen-printed carbon electrode for multiplexed label-free amperometric immuniosensor: addressing its conductivity and

reproducibility challenges, Biosens. Bioelectron. 101 (2018) 304–310.
[25] M. Esajas, J. Duk, H. De-Bruijn, J. Aalders, P. Willemse, W. Sluiter, B. Pras, K. Ten-Hoor, H. Hollema, A. Van-Der-Zee, Clinical value of routine serum squamous cell carcinoma antigen in follow-up of patients with early-stage cervical cancer, J. Clin. Oncol. 19 (2001) 3960–3966.
[26] R.W. Holloway, A. To, M. Moradi, L. Boots, N. Watson, H.M. Shingleton, Monitoring the course of cervical carcinoma with the squamous cell carcinoma serum radio-immunoassay, Obstet. Gynecol. 32 (1990) 293–293.
[27] D. Lu, J. Xia, Z. Deng, X. Cao, Detection of squamous cell carcinoma antigen in cervical cancer by surface-enhanced Raman scattering-based immunoassay, Anal. Methods 11 (2019) 2809–2818.
[28] Y. Li, Y. Zhang, F. Li, J. Feng, M. Li, L. Chen, Y. Dong, Ultrasensitive electrochemical immunosensor for quantitative detection of SCCA using Co3O4@CeO2-Au@Pt nanocomposite as enzyme-mimetic labels, Biosens. Bioelectron. 92 (2017) 33–39.
[29] L. Chen, D. Huang, S. Ren, T. Dong, Y. Chi, G. Chen, Preparation of graphite-like carbon nitride nanoflake film with strong fluorescent and electrochemiluminescent activity, Nanoscale 5 (2013) 225–230.
[30] Y. Wan, Z. Guo, X. Jiang, K. Fang, X. Lu, Y. Zhang, N. Gu, Quasi-spherical silver nanoparticles: aqueous synthesis and size control by the seed-mediated Lee-Meisel method, J. Colloid Interface Sci. 394 (2013) 263–268.
[31] H. Xia, S. Bai, J. Hartmann, D. Wang, Synthesis of monodisperse quasi-spherical gold nanoparticles in water via silver(I)-assisted citrate reduction, Langmuir 26 (2010) 3585–3589.
[32] X. Li, Z. Guo, J. Li, Y. Zhang, H. Ma, X. Pang, B. Du, Q. Wei, Quenched electrochemiluminescence of Ag nanoparticles functionalized g-C_3N_4 by ferrocene for highly sensitive immunosensing, Anal. Chim. Acta 854 (2015) 40–46.
[33] S. Deng, P. Yuan, X. Ji, D. Shan, X. Zhang, Carbon nitride nanosheet-supported porphyrin: a new biomimetic catalyst for highly efficient bioanalysis, ACS Appl. Mater. Interfaces 7 (2015) 543–552.
[34] J. Qin, J. Huo, P. Zhang, J. Zeng, T. Wang, H. Zeng, Improving the photocatalytic hydrogen production of Ag/g-C_3N_4 nanocomposites by dye- sensitization under visible light irradiation, Nanoscale 8 (2016) 2249–2259.
[35] Y. Fu, W. Liang, J. Guo, H. Tang, S. Liu, MoS_2 quantum dots decorated g-C_3N_4/Ag heterostructures for enhanced visible light photocatalytic activity, Appl. Surf. Sci. 430 (2018) 234–242.
[36] H. Chen, H. Zhang, R. Yuan, S. Chen, Novel double-potential electrochemi- luminescence ratiometric strategy in enzyme-based inhibition biosensing for sensitive detection of organophosphorus pesticides, Anal. Chem. 89 (2017) 2823–2829.
[37] B. Xia, Q. Yuan, M. Chu, S. Wang, R. Gao, S. Yang, C. Liu, S. Luo, Directly one-step electrochemical synthesis of graphitic carbon nitride/graphene hybrid and its application in ultrasensitive electrochemiluminescence sensing of pentachlorophenol, Sensor. Actuator. B 228 (2016) 565–572.
[38] C. Cheng, Y. Huang, J. Wang, B. Zheng, H. Yuan, D. Xiao, Anodic electrogenerated chemiluminescence behavior of graphite-like carbon nitride and its sensing for rutin, Anal. Chem. 85 (2013) 2601–2605.
[39] M. Iranifam, Chemiluminescence reactions enhanced by silver nanoparticles and silver alloy nanoparticles: applications in analytical chemistry, Trac. Trends Anal. Chem. 82 (2016) 126–142.
[40] H. Wang, Y. Chai, H. Li, R. Yuan, Sensitive electrochemiluminescent immunosensor for diabetic nephropathy analysis based on tris(bipyridine) ruthenium(II) derivative with binary intramolecular self-catalyzed property, Biosens. Bioelectron. 100 (2018) 35–40.
[41] H. Jia, P. Gao, H. Ma, Y. Li, J. Gao, B. Du, Q. Wei, Ultrasensitive electrochemical immunosensor for squamous cell carcinoma antigen detection using lamellar montmorillonite-gold nanostructures as signal amplification, Talanta 132 (2015) 803–808.
[42] Y. Lin, S. Xu, J. Yang, Y. Huang, Z. Chen, B. Qiu, Z. Lin, G. Chen, L. Guo, Interesting optical variations of the etching of Au Nanobipyramid@Ag Nanorods and its application as a colorful chromogenic substrate for immunoassays, Sensor. Actuator. B 267 (2018) 502–509.
[43] L. Zhao, H. Han, Z. Ma, Improved screen-printed carbon electrode for multiplexed label-free amperometric immuniosensor: addressing its conductivity and reproducibility challenges, Biosens. Bioelectron. 101 (2018) 304–310.
[44] Y. Wu, Y. Zhao, Y. Wang, X. Ye, T. Wu, H. Deng, P. Wu, C. Li, Sensitive immunosensing of squamous cell carcinoma antigen based on a nanocomposite of poly {3-amine-N-[3-(N-pyrrole)propyl]imidazole bromide} ionic liquid and gold nanoroots, Biosens. Bioelectron. 96 (2017) 140–145.